

# Extremely Sub-wavelength Planar Magnetic Metamaterials

Wen-Chen Chen<sup>†</sup>, Christopher M. Bingham<sup>†</sup>, Kelley M. Mak,  
Nicholas W. Caira, and Willie J. Padilla

Department of Physics, Boston College, 140 Commonwealth Ave., Chestnut Hill, MA 02467,  
USA

<sup>†</sup> Contributed equally to this work.

[Willie.Padilla@bc.edu](mailto:Willie.Padilla@bc.edu)

**Abstract:** We present highly sub-wavelength magnetic metamaterials designed for operation at radio frequencies (RFs). A dual layer design consisting of independent planar spiral elements enables experimental demonstration of a unit cell size ( $a$ ) that is  $\sim 700$  times smaller than the resonant wavelength ( $\lambda_0$ ). Simulations indicate that utilization of a conductive via to connect spiral layers permits further optimization and we achieve a unit cell that is  $\lambda_0/a \sim 2000$ . Magnetic metamaterials are characterized by a novel time domain method which permits determination of the complex magnetic response. Numerical simulations are performed to support experimental data and we find excellent agreement. These new designs make metamaterial low frequency experimental investigations practical and suggest their use for study of magneto-inductive waves, levitation, and further enable potential RF applications.

© 2022 Optical Society of America

**OCIS codes:** (160.3918) Metamaterials; (160.3820) Magneto-optical materials; (170.3880) Medical and biological imaging; (260.2160) Energy transfer; (300.0300) Spectroscopy

---

## References and links

1. D. R. Smith, W. J. Padilla, D. C. Vier, S.C. Nemat-Nasser, and S. Schultz, "A composite medium with simultaneously negative permeability and permittivity," *Phys. Rev. Lett.* **84**, 4184–4187 (2000).
2. R. A. Shelby, D. R. Smith, and S. Schultz, "Experimental verification of a negative index of refraction," *Science* **292**, 77–79 (2001).
3. V. G. Veselago "The electrodynamics of substances with simultaneously negative values of  $\epsilon$  and  $\mu$ ," *Sov. Phys. Usp.* **10**, 509–514 (1968).
4. J. B. Pendry, A. J. Holden, D. J. Robbins, and W. J. Stewart, "Magnetism from Conductors and Enhanced Non-linear Phenomena," *IEEE Transactions on Microwave Theory and Techniques* **47** 2075–2084 (1999).
5. D. Schurig, J. J. Mock, B. J. Justice, S. A. Cummer, J. B. Pendry, A. F. Starr, D. R. Smith "Metamaterial electromagnetic cloak at microwave frequencies," *Science* **314**, 977–980 (2006).
6. J. B. Pendry, "Negative refraction makes a perfect lens," *Phys. Rev. Lett.* **85** 18 3966–3969 (2000).
7. D. R. Smith "How to build a superlens" *Science*, **308**, 502 (2005).
8. X. Liu, T. Tyler, T. Starr, A. F. Starr, N. M. Jokerst, and W. J. Padilla, "Taming the blackbody with infrared metamaterials as selective thermal emitters," *Phys. Rev. Lett.* **107**, 045901 (2011).
9. T. J. Yen, W. J. Padilla, N. Fang, D. C. Vier, D. R. Smith, J. B. Pendry, D. N. Basov, X. Zhang, "Terahertz Magnetic Response from Artificial Materials," *Science* **303** 1494–1496 (2004).
10. S. Linden, C. Enkrich, M. Wegener, J. Zhou, T. Koschny, and C. M. Soukoulis, "Magnetic Response of Metamaterials at 100 Terahertz," *Science* **306** 1351–1353 (2004).
11. C. Enkrich, M. Wegener, S. Linden, S. Burger, L. Zschiedrich, F. Schmidt, J. F. Zhou, Th. Koschny, and C. M. Soukoulis, "Magnetic Metamaterials at Telecommunication and Visible Frequencies," *Phys. Rev. Lett.* **95** 203901 (2005).

12. E. Shamonina, V. A. Kalinin, K. H. Ringhofer, and L. Solymara "Magnetoinductive waves in one, two, and three dimensions," *J. Appl. Phys.* **92** No.10 6252–6261 (2002).
13. M. C. K Wiltshire, "RF metamaterials," *Phys. Status Solidi B-basic Solid State Phys.* **224** 1227–1236 (2007).
14. S. Tricarico F. Bilotti L. Vegni "Multi-functional dipole antennas based on artificial magnetic metamaterials," *IET Microwave Antennas Propag.*, **4** Iss.8 1026–1038 (2010).
15. F. Paredes, G. Z. Gonzalez, J. Bonache, F. Martin, "Dual-band impedance-matching networks based on splitting resonators for applications in RF identification (RFID)," *IEEE Trans. on Microwave Theory and Tech.* **58** 1159–1166 (2010).
16. M. C. K Wiltshire, J. V. Hajnal, J. B. Pendry, et al. "Metamaterial endoscope for magnetic field transfer: near field imaging with magnetic wires," *Opt. Express* **11** Issue:7 709–715 (2003).
17. J. D. Baena, R. Marques, F. Medina, and J. Martel, "Artificial magnetic metamaterial design by using spiral resonators," *Phys. Rev. B* **69**, 014402 (2004).
18. M. J. Freire, R. Marques, "Planar magnetoinductive lens for three-dimensional subwavelength imaging," *Appl. Phys. Lett.* **86** iss:18 182505 (2005).
19. Yaroslav Urzhumov and David R. Smith, "Metamaterial-enhanced coupling between magnetic dipoles for efficient wireless power transfer," *Phys. Rev. B* **83** 205114 (2011)
20. B. Wang, K. H. Teo, T. Nishino, W. Yezazunis, J. Barnwell, and J. Zhang, "Experiments on wireless power transfer with metamaterials," *Appl. Phys. Lett.* **98** 254101 (2011)
21. Filiberto Bilotti, Alessandro Toscano, and Lucio Vegni, "Design of Spiral and Multiple Split-Ring Resonators for the Realization of Miniaturized Metamaterial," *IEEE Trans. Antennas Propag.* **55** NO. 8 (2007).
22. C. Kurter, J. Abrahams; S. M. Anlage, "Miniaturized superconducting metamaterials for radio frequencies," *Appl. Phys. Lett.* **96** Issue:25 253504 (2010)
23. R. Marque, F. Mesa, J. Martel, and F. Medina, "Comparative analysis of edge- and broadside-coupled split ring resonators for metamaterial design - Theory and experiments," *IEEE Trans. Antennas Propag.* **51** Issue: 10 2572–2581 (2003).
24. D. R. Smith, D. C. Vier, Th. Koschny, and C. M. Soukoulis, "Electromagnetic parameter retrieval from inhomogeneous metamaterials," *Phys. Rev. E* **71** , 036617 (2005).

---

## 1. Introduction

Experimental verification of a negative index of refraction[1, 2] confirmed a four decade old theoretical prediction[3] and initiated a new area of research in artificial electromagnetic (EM) materials[4], known as metamaterials (MMs). In the last decade metamaterials research has yielded many exotic effects including: invisibility cloaking[5], perfect lensing[6, 7], and perfect absorbers[8]. Interest in metamaterials stems from their available use in nearly any band of the electromagnetic spectrum and their ability to achieve almost any desired electromagnetic response[9, 10, 11].

While there are relatively few technical restrictions limiting operational frequencies of metamaterials there are, however, some practical hurdles. To date there has been a noticeable lack of metamaterials demonstrated at low frequencies – on the order of 100 MHz or lower. Traditional RF devices in use today cover a number of disciplines ranging from long range satellite communication, magnetic resonance imaging (MRI), to common everyday devices like radios and televisions. Although metamaterials may offer advantages to the above mentioned devices, the main drawback is that the dimensions can become impractically large. Wavelengths for these frequencies range from thousands of meters (for 100's kHz) to lengths of meters (100's MHz). Since it is not uncommon for individual metamaterial elements to have sizes on the order of  $\sim \lambda_0/10 - \lambda_0/100$ , (where  $\lambda_0$  is free space wavelength at resonance), the side length of a single RF metamaterial element could be expected be around 100 m to 10 cm. In many situations this size may be unacceptable for real-world applications, particularly so for 'portable' devices. The development of a new class of metamaterials with a significant reduction in the ratio of its physical size 'a' to its resonant wavelength  $\lambda_0$  may create new opportunities for low frequency metamaterial-based applications[12, 13, 14, 15].

Magnetic properties exhibited by natural materials are typically weaker and less common than their electric counterpart. This is due to the fundamental difference in how magnetic and electric responses are generated - the former being produced either from orbital currents or

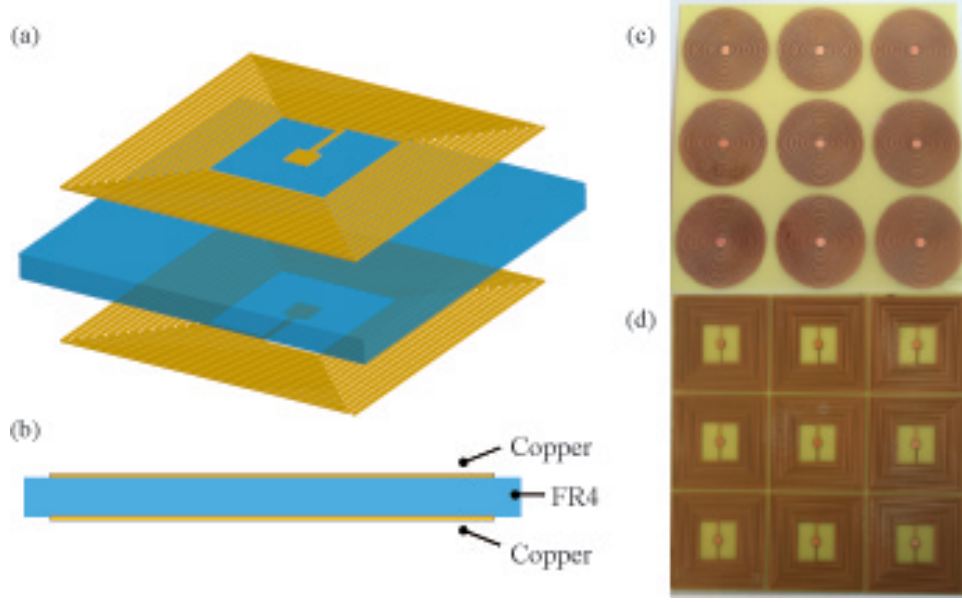


Fig. 1. (a) Schematic (exploded view) of the dual-layer square spiral metamaterial. (b) Side view showing material layers. Photographs of fabricated metamaterial circular spirals (c) and square spirals (d).

intrinsic unpaired spins. This fundamental lack of diversity in materials hinders full development of electromagnetic devices. Metamaterials with a  $\mu$ -negative response have been shown to improve the effectiveness of systems that make use of magnetic fields at radio frequencies such as increasing the resolution of an MRI[16, 17, 18] and enhancing wireless power transfer efficiency[19, 20].

Here we propose that dual layer metamaterial spirals may be used in order to achieve extremely sub-wavelength RF magnetic metamaterials. We utilize and detail a time domain method for characterization of the complex magnetic response ( $\mu(\omega)$ ) of the RF metamaterials and support experimental results with simulation.

## 2. Spiral Metamaterial Design and Simulations

As a starting point for exploration of RF magnetic metamaterials we begin with a design based on a planar spiral structure capable of achieving large inductances[21, 22] – as it is trivial to wind a significant length of wire into a small area. The spiral response can be approximated based on a simple  $LC$  resonator model  $\omega_0 = 1/\sqrt{LC}$ , where  $\omega_0$  is the resonant angular frequency.  $L$  is the inductance, and  $C$  is the capacitance of the MM. Additional reduction of the unit cell size may thus be achieved by maximizing  $L$  and  $C$  simultaneously. In single layer planar spirals the capacitance arises solely due to interactions between adjacent metallic windings - the so-called ‘edge coupling’ capacitance[23]. However, since typical lithographic methods produce extremely thin metallic layers the capacitive values obtained in this manner are small. We may drastically increase the capacitance by adding a second spiral layer, thus creating an interlayer interaction between the two planar structures. In this way both the larger area of the broadside metallic surfaces and a supporting dielectric in-between will provide an increased capacitance. A similar idea had been demonstrated in the microwave range, “the broadside-

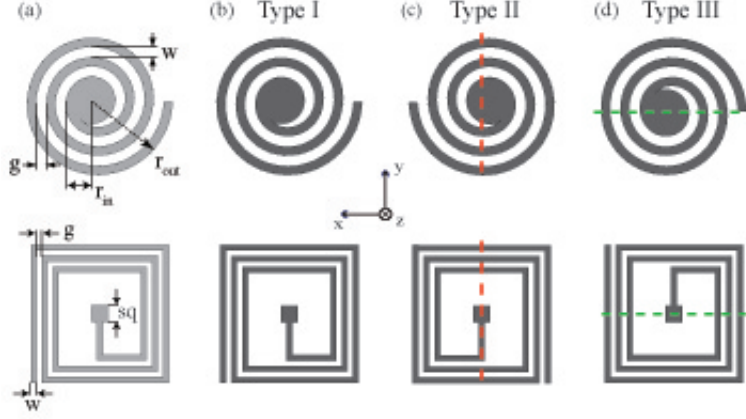


Fig. 2. Schematic illustrating the geometry of circular (top row) and square (bottom row) spiral metamaterials. In the top of (a) the notation used for description of the geometry is shown. Column (a) shows the single layer structure, and (b), (c) and (d) show the orientation of the second spiral layer in type I, II, and III structures, respectively, as described in the text.

coupled” SRR was found to have a resonance occurring at much lower frequency than the original single layer design[23]. The addition of the second layer will also provide an enhancement of the metamaterial inductance - so long as the inductances are added in series.

We investigate two different varieties of the planar spiral – circular and square windings. For each we consider three independent dual-layer configurations, termed as types I, II, and III. The paired spirals in each configuration represent different symmetry operations between layers. If we define a coordinate system that is centered in the middle of the two metallizations in the  $z$ -direction and centered laterally and horizontally, then the type I spirals, Fig. 2 (b), have two identical structured patterns on top and bottom layers, where the top layer is simply translated along the  $z$ -axis by some distance  $d$ . In Fig. 2 (c) we show the type II case where the top and bottom layers have 180 degree rotational symmetry about the  $y$ -axis. In the type III case the top and bottom layers have 180 degree rotational symmetry about the  $x$ -axis. In all cases, metallic layers on each side of the substrate are capacitively coupled through a circular or square pad located in the center of the unit cell.

Simulations were performed with a commercially available 3D full wave finite element frequency domain solver. Excitation from a waveguide port is used where the electric field is along the  $x$  direction, and the magnetic field is along the  $z$ . The simulated circular spiral design has: 21 turns, a linewidth  $w = 170 \mu\text{m}$ , line spacing  $g = 320 \mu\text{m}$ , inner radius  $r_{in} = 1.2 \text{ mm}$ , outer radius  $r_{out} = 11.7 \text{ mm}$ , and unit cell size of  $25.4 \text{ mm}$ . The square spiral has: 13 turns, a linewidth  $w = 210 \mu\text{m}$ , line spacing  $g = 320 \mu\text{m}$ , side length of the central capacitive pad  $sq = 1.9 \text{ mm}$ , and the side length of the square coil is  $25 \text{ mm}$  with a unit cell size of  $26 \text{ mm}$ . The dielectric slab for both patterns is  $203 \mu\text{m}$  thick and was modeled using a dielectric value of  $2.6 + 0.04i$ . All metallic components were modeled as copper with a conductivity of  $\sigma = 5.8 \times 10^7 \text{ S/m}$ . In all cases the geometry of the spiral, including the size of the centrally located capacitive pad, was modified in order to obtain the greatest oscillator strengths. The effective permeability  $\mu_r$  for each metamaterial design was extracted from the simulated complex scattering parameters[24].

The extracted permeability for each magnetic metamaterial is shown in Fig. 3 (a) for the circular spirals and Fig. 3 (b) for the square spirals. A single layer spiral design (Fig. 3 blue

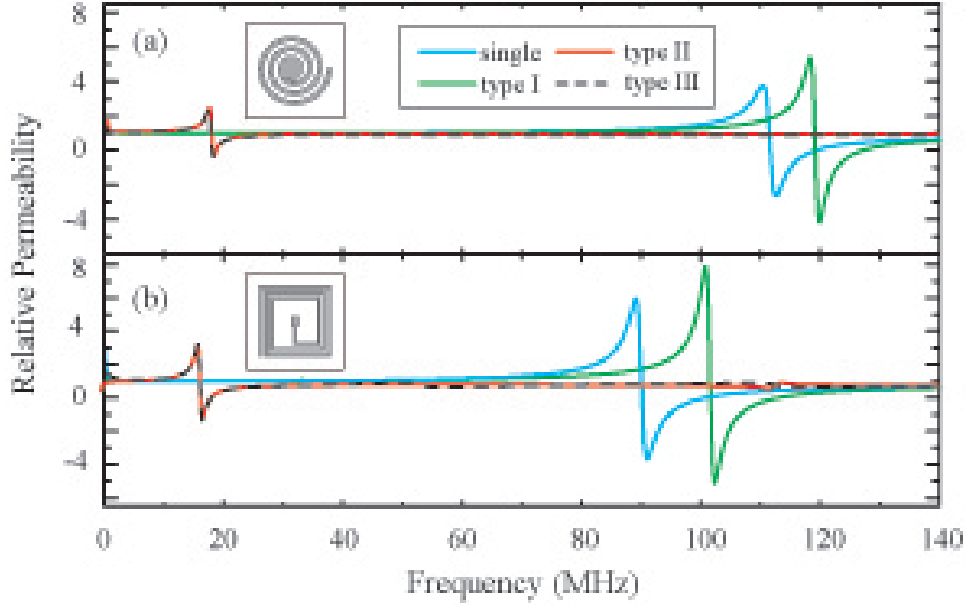


Fig. 3. Simulated permeability of several different types of spiral metamaterials, the single-layer (blue curves), type I (green curves), type II (red curves), and type III (dash black curves).

curve) was examined to act as a reference point for the dual layer structures. A prominent magnetic Lorentzian type resonance can be observed for each configuration described by,

$$\tilde{\mu}_r = \mu_\infty + \frac{\omega_{mp}^2}{\omega_0^2 - \omega^2 - i\gamma\omega} \quad (1)$$

where  $\mu_\infty$  is the relative permeability at frequencies higher than the resonance,  $\omega_{mp}$  is the magnetic plasma frequency,  $\omega_0$  is the center frequency of the resonance, and  $\gamma$  is the loss. In Table I we list the parameters for a Lorentz oscillator fit to the simulated magnetic response - the resonant frequency ( $\omega_0$ ), minimum  $\mu$  value, the oscillator strength ( $\omega_{mp}/2\pi$ ), and the resonant wavelength to unit cell size ratio ( $\lambda_0/a$ ). In the single layer case the resonance of the circular (c) and the square (s) spirals occur at frequencies of 112 MHz and 90 MHz. They both have good oscillator strength with values of 40 MHz for both. For the type I design (green curves of Fig 3),  $\mu$ -resonances shifted to higher frequencies by approximately 10%, compared to the single layer spirals, for both circular and square designs. Resonant frequencies for both type II and III configurations lie below 20 MHz and simulated oscillator strengths for these designs are lower than the single layer spiral and type I structures. It is clear, however, that Type III circular and square designs achieve the largest  $\lambda_0/a$  values and thus we have chosen to experimentally investigate these particular structures.

### 3. Magnetic Time Domain Spectroscopy

In order to characterize the complex permeability ( $\tilde{\mu}(\omega) = \mu_1 + i\mu_2$ ) response of our magnetic metamaterials, ( $\mu_1$  and  $\mu_2$  are the real and imaginary portions of the magnetic response function, respectively), we utilized a time-domain spectroscopic method. A schematic illustrating our experimental apparatus is shown in Fig. 4. In our setup a driving coil, (bottom of Fig. 4), is

Table 1. Parameter values from fits to simulated  $\mu_r$  for the circular and the square metamaterials shown in Fig. 3.

| Type         | $\omega_0/2\pi$ (MHz) | $\mu_{min}$ | $\omega_{mp}/2\pi$ (MHz) | $\lambda_0/a$ |
|--------------|-----------------------|-------------|--------------------------|---------------|
| (C) single   | 112                   | -2.64       | 40                       | 105           |
| (C) type I   | 119                   | -4.20       | 41.7                     | 99.3          |
| (C) type II  | 17.8                  | -0.342      | 5.5                      | 664           |
| (C) type III | 17.3                  | -0.357      | 5.8                      | 683           |
| (S) single   | 90.2                  | -3.97       | 40.4                     | 131           |
| (S) type I   | 101                   | -5.11       | 46.2                     | 116           |
| (S) type II  | 16.8                  | -1.51       | 6.95                     | 703           |
| (S) type III | 16.7                  | -1.52       | 6.98                     | 707           |

driven by a voltage pulse from a function generator creating a transient magnetic field. A second coil (pickup coil) is co-axially aligned with the drive coil, (spaced a distance  $z$  away) and measures the induced time dependent electromotive force ( $emf(t)$ ) due to the incident magnetic field created by the drive coil. Based on the Faraday's law of induction, the induced  $emf$  can be described as,

$$emf(t) = -\frac{d\Phi_B}{dt} \quad (2)$$

where  $\Phi_B$  is the magnetic flux defined as,

$$\Phi_B = \int \mathbf{B} \cdot d\mathbf{A} \quad (3)$$

For a magnetic field component in the vertical ( $z$ -axis) direction at the pickup coil of  $B_z$  and an assumed time harmonic dependence ( $\mathbf{B} \sim e^{-i\omega t}$ ), we may thus write the  $emf$  as,

$$emf(t) = -A\mu_r\mu_0 \frac{dH_z}{dt} \quad (4)$$

where  $A$  is the area of the pickup coil, and we have used  $\mathbf{B} = \mu\mathbf{H} = \mu_r\mu_0\mathbf{H}$ .

In order to determine the complex permeability of a magnetic material we perform a referenced time domain measurement. This is achieved by first characterizing the response of the apparatus with no materials present, i.e. we measure a reference electromotive force of  $emf(t)_r \equiv -A\mu_0 dH_z/dt$ , since  $\mu_r = 1$  for free space. We then place a planar material which has an area  $A$  into the pickup coil and characterize its time dependent electromotive force as  $emf(t)_s \equiv -A\mu_r\mu_0 dH_z/dt$ . Thus by taking the ratio of the time dependent  $emf$ 's we are able to characterize the complex frequency dependent permeability as,

$$\tilde{\mu}_r(\omega) = \left\{ \frac{\hat{F}(emf(t)_s)}{\hat{F}(emf(t)_r)} \right\} \quad (5)$$

where  $\hat{F}$  stands for the complex Fourier transform. It's worth noting that there are no restrictions on homogeneity of the magnetic field and for the case where  $\mathbf{B}$  has a high spatial dependence the extraction method described in Eq. 5 is still valid. We use the time domain method described here to characterize the complex magnetic response of metamaterials. In all cases we have made the areas of the pickup coil and metamaterial samples equal.

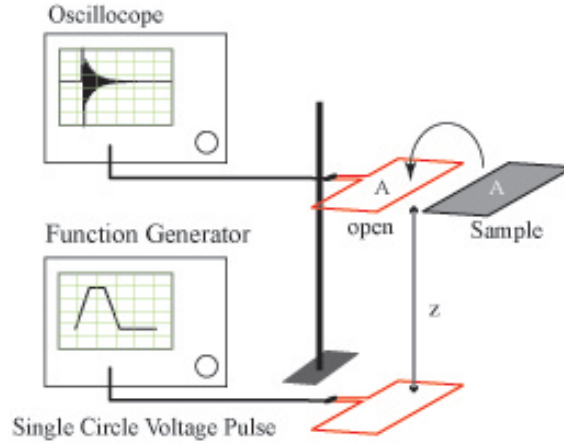


Fig. 4. Schematic of the experimental apparatus as described in the text.

#### 4. Fabrication and Characterization

Metamaterial samples were fabricated using printed circuit board (PCB) photolithography. We used a dual sided copper clad FR4 board (thickness of  $203 \mu\text{m}$ ) where both metallization were  $17 \mu\text{m}$  thick. A photomask for the square spiral geometry was created by printing on a transparency with a standard high resolution laser printer. For the circular spiral geometry a transparency mask was purchased from a commercial vendor. After the board was exposed to UV light through the photomask, a ferric chloride bath was used to etch away the unwanted copper to create patterned spiral metamaterials. The dimensions of both the circular and square geometries are identical to those in the computational models. Optical images of a unit cell of the fabricated samples are shown as insets to Fig. 1 (c) (circular spiral) and (d) (square spiral).

The time dependent magnetic field used to characterize our metamaterial samples was generated using a coil antenna driven by a transient voltage. The peak to peak voltage ( $V_{pp}$ ) was set to 10 V at a frequency of 12.5 MHz with a duty cycle of 37.5%. A receiving coil spaced a distance of 8 cm away was connected to a digital sampling oscilloscope which captured the time dependent electromotive force induced by the incident magnetic flux. The shape and dimensions of the receiving coil were chosen such that it matched that of a  $3 \times 3$  array of our magnetic metamaterials. For each sample we performed two measurements. The first was a reference where nothing was placed inside the receive coil. For sample characterization we placed the metamaterial array into the center of the receiving coil. All measurement were collected with an average of 128 wave forms.

Representative time pulses are shown in Fig. 5 (a) for both the sample (black curve) and reference measurement (red curve). A noticeable difference can be seen between the two measured time pulses as the reference signal has almost completely died out after 600ns, while the metamaterial signal ‘rings’ for a much longer time (over 1800ns). A plot of the frequency spectra calculated from the Fourier transform of the time data is shown in Fig. 5 (b). Applying the extraction method of Eq. 5, outlined earlier, one can determine the effective permeability  $\mu_r$  of the magnetic metamaterials. Due the dimensions of our antenna coils and the input time signal characteristics the useable spectral range was 3-30 MHz.

The real and imaginary portions of the measured permeability of the samples are plotted as black curves in Fig. 6 for both the circular (top panels) and square type III (bottom panels)

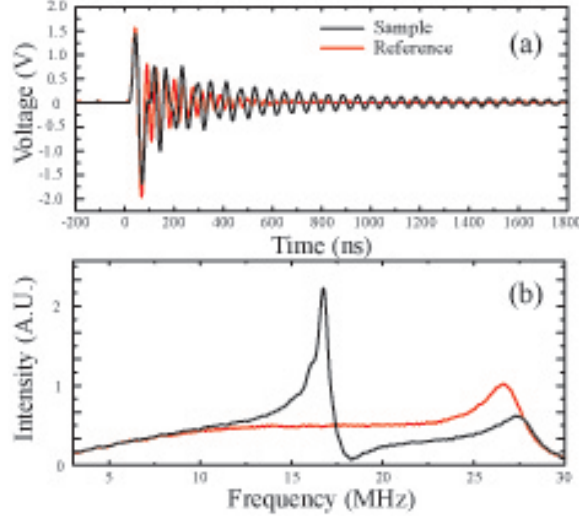


Fig. 5. (a) Time domain waveform recorded by the pickup coil for the metamaterial (black curve) and a reference signal (red curve). The amplitude spectrum for the metamaterial (black) and reference (red) obtained by a Fourier transformation of (a).

samples. As can be observed both spiral metamaterial structures yield magnetic resonances with Lorentz-like lineshapes. The circular spiral has its resonance centered at 17.3 MHz and the square spiral at 16.8 MHz. The real part of the measured relative permeability for both designs reaches a negative value of -0.25 for the circular design and -1.51 for the square design. The full width at half maximum (FWHM) is 0.554 (MHz) and 0.794 (MHz) for the circular and square designs, respectively. The calculated Q-factors are 30.3 and 21.8, which shows both designs have the decent oscillator strength at the resonances.

The simulated results of the type III spirals are as displayed as dashed red curves in Fig. 6. In comparison to the experimental results (black solid lines), the simulated curves are nearly identical to the measured ones. For example the simulated and experimental peak  $\mu$  values differ by only 0.2% and 0.1% for the square and circular spirals, respectively. Some discrepancies in the amplitudes and  $\Delta f$  for both designs are observed. Nevertheless, the experiments are in excellent agreement with the simulations. The errors are most likely be attributed to imperfections from the fabrication process.

We compared experimental permeabilities to a frequency-dependent Drude-Lorentz oscillator, as shown in Eq. 1. The grey curves of Fig. 6 are fits to the experimental data and we find good agreement with parameters of:  $\mu_\infty = 0.893$ ,  $\omega_{mp} = 2\pi \times 4.91$  (MHz),  $\gamma = 2\pi \times 0.745$  (MHz), and  $\omega_0 = 2\pi \times 17.3$  (MHz) for the circular geometry, and  $\mu_\infty = 0.87$ ,  $\omega_{mp} = 2\pi \times 6.6$  (MHz),  $\gamma = 2\pi \times 0.587$  (MHz), and  $\omega_0 = 2\pi \times 16.8$  (MHz) for the square geometry.

## 5. Discussion

Radio frequency magnetic metamaterials investigated here yield reasonably strong resonances although their physical size ( $a$ ) is only a small fraction of their resonant wavelength. Circular spiral metamaterials achieved  $a = \lambda_0/683$  and square designs  $a = \lambda_0/703$ . Resonant wavelengths of Type II and III designs are nearly six times smaller than  $\lambda_0$  obtained from single layer spirals, although all have roughly the same unit cell size. It's worth noting that in spite of the strong sub-wavelength sizes of metamaterials presented here, there are simple improve-



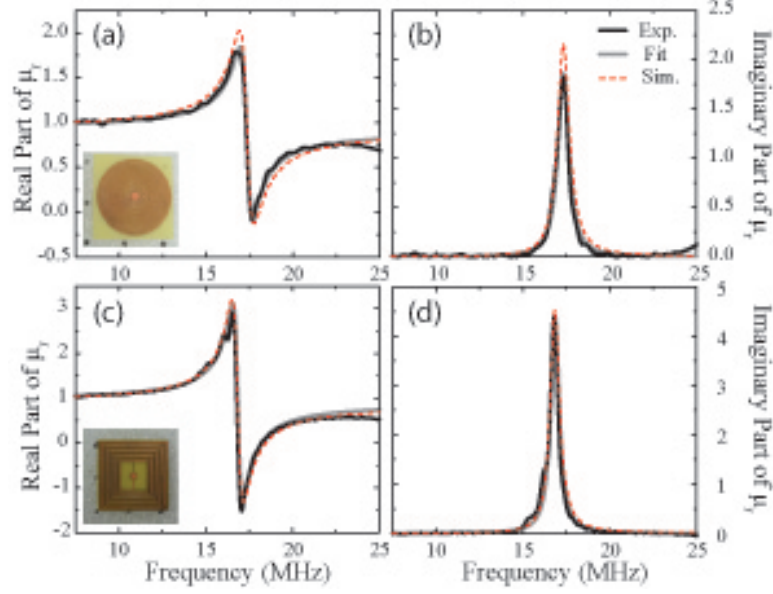


Fig. 6. Experimental (black curves), simulated (dashed red curves) and fits (gray curves) to the real (a,c) and imaginary (b,d) parts of  $\mu_r$ . Panels (a) and (b) show the real and imaginary permeability, respectively, for the circular spiral. Panels (c) and (d) show the real and imaginary permeability, respectively, for the square spiral.

ments which will further increase  $\lambda_0/a$ . For example we have chosen to fabricate designs in which the two planar spirals are independent and are only capacitively coupled through the substrate. We chose this geometry simply because these structures are easier to fabricate, however by connecting the two layers with a conductive via one may push sizes of these structures even more sub-wavelength, as the unwound length effectively doubles.

Figure 7 presents simulations of a type III square spiral, with a connecting via, and a unit cell size  $a = 15.5$  mm, linewidth  $w = 100$   $\mu\text{m}$ , line spacing  $g = 100$   $\mu\text{m}$ , board thickness of 203  $\mu\text{m}$ , and consisting of 25 windings. Simulations indicate this design should exhibit a strong magnetic resonance at 9.34 MHz and the extracted complex  $\mu$  is shown in Fig. 7 (a). For this geometry we thus find  $a = \lambda_0/2072$ . Although the design discussed above is well within both laboratory and commercial fabrication capabilities, here we chose to experimentally demonstrate a slightly less subwavelength structure, and simply modify the type III circular spiral shown in Fig. 1 (a) and (c). Holes were drilled through the center capacitive pad of each unit cell and a wire was soldered on both sides to create the connecting via. We then characterized the sample and extracted the complex permeability as shown in Fig. 7 (b). We find a resonant frequency of 8.94 MHz and thus this modified spiral magnetic metamaterial yields  $a = \lambda_0/1321$ . It should be noted that the experimental structure presented here was by no means an optimized design, i.e. we did not optimize capacitive and inductive reactances which could be responsible for the significantly lowered oscillator strength. Additionally a significant Ohmic loss resulted from the manner in which the conductive via was experimentally implemented. The metamaterial geometry was simulated where the via was modeled as a resistive element ( $R=13\Omega$ ) and we find excellent agreement with experiment as shown in Fig. 7 (b).

Although the measured magnetic responses shown in Fig. 6 and 7 are well described by Lorentz oscillators, careful consideration of the assignment of  $\mu_r(\omega)$  to metamaterials studied

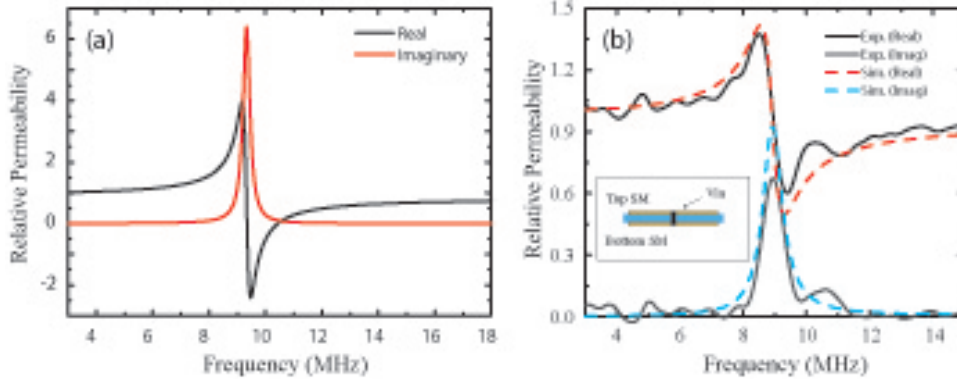


Fig. 7. (a) Simulated real (black) and imaginary (red) relative permeability for a dual layer circular spiral metamaterial with an interlayer via. (b) Experimental (solid curves) and simulated (dashed curves) relative permeability of a type III circular spiral metamaterial with conductive via - described in the text.

here should be given. As the permeability is equal to the number of magnetic dipoles per unit volume – and our metamaterials consist of only a single layer – one might by extension assume that metamaterials should consist of multiple layers in order to be appropriately described by effective optical constants. In this case it is clear that any response which results due to incident time varying magnetic fields, must happen within the physical bounds of the metamaterial. More specifically in the case of the magnetic metamaterials investigated here, this can only be a re-arrangement of electrons within the conductive spiral itself. Thus we take as the volume as  $0.237\text{mm} \times a \times a \sim 150\text{mm}^3$ . However it is important to note that the response fields significantly extend beyond the physical thickness and, in the direction normal to the plane, are only negligible at some distance ( $D$ ) away. Thus any material placed within  $D$  will effect the response of the metamaterial and thus alter  $\mu_r$ . This is not, however, a barrier to specifying a unique permeability to metamaterials, so long as metamaterials are spaced a distance  $D$  apart in the  $z$  direction.

If this is true then measured  $\mu_r$  values should be independent of the apparatus and the particular spacing between the pickup and drive coils used. In simulations (not shown) we investigated the dependence of the resonant frequency of a spiral metamaterial and dimensions of the bounding box along the direction normal to the metamaterial plane. As the size of the bounding box increases, the resonant frequency also increases but eventually asymptotes to some value ( $\omega_0$ ). Computational investigations indicate that for both square and circular type III geometries the resonant wavelength saturates when the side length of the bounding box is around 40mm. At this distance the fields of the metamaterial are small enough that anything place beyond this distance will not affect the response.

As a verification to the validity of the experimental time-domain method presented here, we performed measurements of the response of magnetic metamaterials for several coil separation distances ranging from  $z = 4$  cm to  $z = 24$  cm. In all cases the sample under investigation was placed directly in the plane of the pick-up coil. As before all sample measurements were characterized and compared with a reference measurement. The induced maximum peak-to-peak value of the *emf* for the reference measurements was observed to change from 2V for the closest spacing to 40 mV for the farthest. Calculated  $\mu_r$  values are shown for three characteristic separations of  $z=8, 16$ , and  $24$  cm in Fig. 8 (a). In Fig. 8 (b) and (c) we plot, respectively, the peak-to-valley amplitude of  $\mu_r$  and the resonance frequency  $\omega_0$ , both as a function of coil

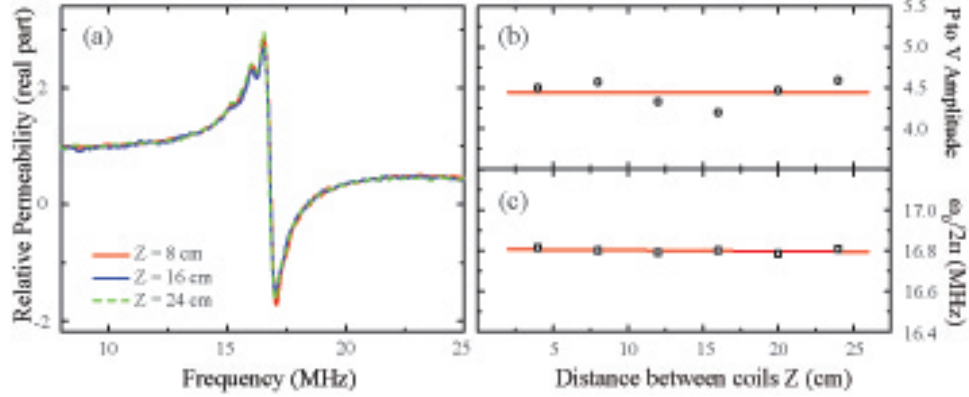


Fig. 8. (a) Measured permeability for several values of coil separation  $z$ . The peak to valley amplitude of  $\mu_r$  (b) and the resonant frequency ( $\omega_0/2\pi$ ) (c) versus the coil separation distance ( $z$ ). Solids red lines are linear fits to the data.

separation. The red horizontal lines of Fig. 8 (b,c) are fits to the data and have nearly zero slope to within  $10^{-4}$ . The measured center frequencies only deviate by a maximum of 1% of the average value for  $z$  distances studied here. Variation, however, in the peak-to-valley  $\mu_r$  values is as much as 5% though we attribute this discrepancy to noise in the system.

## 6. Conclusion

We computationally and experimentally demonstrated extremely sub-wavelength planar magnetic metamaterials. Experimental resonant wavelength to unit cell size values were shown to be as much as  $\sim 1300$ , and an ideal simulated design was shown to be  $\lambda_0/a \sim 2000$ . We find excellent agreement between experimental and simulated magnetic permeabilities, for all structures investigated, and attain reasonable oscillator strengths. A novel characterization method has been presented capable of determining the complex magnetic response of planar material at RFs. Compact sub-wavelength designs presented here make low-frequency study of metamaterial practical which may lead to RF metamaterial applications.

## 7. Acknowledgments

We acknowledge support from the Department of Energy under grant DE-SC0002554. The authors would also like to thank the D. R. Smith and Y. A. Urzhumov for useful discussions.